

# A Determination of the Spectral Index of Galactic Synchrotron Emission in the 1-10 GHz range

**P.Platania<sup>1</sup>, M.Bensadoun<sup>2</sup>, M.Bersanelli<sup>1</sup>, G.De Amici<sup>3</sup>, A.Kogut<sup>4</sup>, S.Levin<sup>5</sup>,  
D.Maino<sup>6</sup>, G.F.Smoot<sup>2</sup>**

<sup>1</sup> Istituto di Fisica Cosmica, Consiglio Nazionale delle Ricerche, via Bassini 15, 20133 Milano, Italy

<sup>2</sup> Space Science Laboratory and Lawrence Berkeley Laboratory, M/S 50-205, University of California, Berkeley CA 94720, USA

<sup>3</sup> TRW, Space and Technology Division, R1 - 2136, 1 Space Park, Redondo Beach CA 90278, USA

<sup>4</sup> Hughes STX, Code 685, NASA/GSFC, Greenbelt MD 20771, USA

<sup>5</sup> Jet Propulsion Laboratory, Pasadena CA 91109, USA

<sup>6</sup> SISSA, International School for Advanced Studies, Strada Costiera 11, 34014, Trieste, Italy

**DRAFT**

( 22-JULY-1997 )

**ABSTRACT** — We present an analysis of simultaneous multifrequency measurements of the Galactic emission in the 1-10 GHz range with  $18^\circ$  angular resolution taken from a high altitude site. Our data yield a determination of the synchrotron spectral index between 1.4 GHz and 7.5 GHz of  $\alpha_{syn} = 2.81 \pm 0.16$ . Combining our data with the maps from Haslam et al. (1982) and Reich & Reich (1986) we find  $\alpha_{syn} = 2.76 \pm 0.11$  in the 0.4 - 7.5 GHz range. These results are in agreement with the few previously published measurements. The variation of  $\alpha_{syn}$  with frequency based on our results and compared with other data found in the literature suggests a steepening of the synchrotron spectrum towards high frequencies as expected from theory, because of the steepening of the parent cosmic ray electron energy spectrum. Comparison between the Haslam data and the 19 GHz map (Cottingham 1987) also indicates a significant spectral index variation on large angular scale. Addition quality data are necessary to provide a serious study of these effects.

## 1 Introduction

The detailed study of continuous radio emission allows a direct evaluation of some important parameters that describe the dynamics and structure of the Galaxy: the mean intensity of the magnetic field, the spectral index of the energy spectrum of cosmic ray electrons and the temperature and density of interstellar clouds. Additional strong motivation for systematic studies of the diffuse Galactic emission arises in conjunction with measurements of the CMB (Cosmic Microwave Background): Galactic emission is one of the main sources of unwanted signal in CMB observations, and it is unavoidable even in satellite measurements. It is then very important to understand in detail the spectral and spatial variations of the various components of Galactic emission in order to separate them from those due to the CMB. For this purpose an experiment dedicated to measuring the low-frequency Galactic emission with multifrequency measurements has been carried out in 1988 from White Mountain, California, as part of a USA-Italy collaboration for measuring the spectrum of the CMB in the Rayleigh-Jeans region (Smoot et al. 1985). In this paper we present these previously unpublished data; because of the lack of Galactic emission surveys in this frequency range, new results in this field are very important.

### 1.1 The Galactic emission

At frequencies lower than  $\sim 30$  GHz Galactic emission is mainly due to synchrotron emission from cosmic ray electrons interacting with the Galactic magnetic fields and to thermal bremsstrahlung (free-free) emission. In the frequency range of our experiment (1-10 GHz) the dominant contribution comes from synchrotron radiation (Fig. 1), with free-free radiation contributing  $\sim 30 - 50\%$  on the Galactic plane. Our first goal is to determine a mean synchrotron spectral index and its possible variation with frequency. The synchrotron emission arises from relativistic cosmic ray electrons moving in the Galactic magnetic fields; for an electron population with energy distribution  $N(E)$  described by a power law

$$N(E)dE \sim E^{-\delta}dE \quad (1)$$

the ensemble synchrotron radiation spectrum in terms of brightness temperature is also a power law

$$T(\nu) \sim \nu^{-\alpha} \quad (2)$$

where  $\nu$  is the radiation frequency and  $\alpha = (\delta + 3)/2$ . In the energy range  $2 \lesssim E \lesssim 15$  GeV (corresponding to frequencies between 408 MHz and 10 GHz) the spectral index of the energy distribution of the cosmic rays electrons is  $\delta \sim 3$  and then  $\alpha \sim 3$ . For higher electron energies, the energy spectrum steepens and so does the radiation spectrum (Banday & Wolfendale 1991).

The brightness temperature distribution depends on the electron density along the line of sight  $N(E, l)$  and on the power  $P$  emitted by an electron of energy  $E$  into a magnetic field  $B$

$$T(\nu) \sim \int \int P(\nu, B, E) N(E, l) dE dl \quad (3)$$

Because of the dependence of  $B$  and  $N(E)$  with the position in the Galaxy, one expects  $T$  and  $\alpha$  to be also functions of the position in the sky.

## 2 The Experiment

Our analysis is based upon a set of data collected during three nights (6, 8, 10 September 1988), from the White Mountain Barcroft Station, California (altitude 3800 m, latitude  $+37^\circ.5$ ; hereafter WM; for a review of the entire experiment campaign see Smoot et al. 1985) with radiometers operating at 1.375, 1.55, 3.8 and 7.5 GHz (Table 1). The instruments are total power radiometers, whose output signal,  $S$ , is proportional to the power,  $P$ , entering the antenna aperture. The two lower frequencies were covered by a single radiometer (Bensadoun et al. 1993) which could switch the center frequency of its YIG filter. Details on the 3.8 and 7.5 GHz radiometer can be found in De Amici et al. 1990 and Kogut et al. 1990. Hereafter the signals are expressed in units of antenna temperature  $T_A = P/kB$ , where  $P$  is the received power,  $k$  is the Boltzmann's constant and  $B$  is the bandwidth of the radiometer.

During the Galactic scans, each radiometer was tipped  $15^\circ$  to the East and  $15^\circ$  to the West of the zenith, measuring the signal from the sky for 32 seconds in each position. We took the difference of the signal in these two positions; in this way we were able to cancel, at first order, all the isotropic contributions (the CMB and the extragalactic sources) and those which give symmetric contributions with respect to the zenith angle (the atmospheric and ground emissions). (We consider the CMB as isotropic, since the CMB dipole contribution in the observed region is negligible, less than 2 mK). The differenced signal can thus be written:

$$T_{A,+15^\circ} - T_{A,-15^\circ} \simeq \Delta T_{A,Gal} + \delta T \quad (4)$$

where  $\delta T$  includes the second-order contributions from the other terms and  $\Delta T_{A,Gal}$  is the sum of differential ( $\pm 15^\circ$ ) synchrotron ( $\Delta T_{A,syn}$ ) and free-free ( $\Delta T_{A,ff}$ ) emissions relative to the observed sky regions:

$$\Delta T_{A,gal} = \Delta T_{A,syn} + \Delta T_{A,ff} \quad (5)$$

For each night we observed for several hours (see Table 1), thus covering significant sections of the sky, with some overlap and redundancy for checking systematic effects.

Calibration measurements were done every hour during the experiment using the signal from an ambient temperature load (typically  $T_{A,amb} \sim 300$  K) and the zenith sky ( $T_{A,zenith} \sim 4$  K). The calibration constant  $G$  is

$$G = \frac{T_{A,amb} - T_{A,zenith}}{S_{amb} - S_{zenith}} \quad (6)$$

where  $T_{A,amb}$  and  $S_{amb}$  are the temperature and the signal when the radiometer is looking at the ambient load and  $T_{A,zenith}$  and  $S_{zenith}$  the temperature and the signal when it looks to the zenith sky. We calibrated the differential signals between the  $15^\circ$  E and  $15^\circ$  W positions using the value of  $G$  resulting from the interpolation between two calibration measurements.

### 3 Data Analysis

The integration time is 2 seconds for all the radiometers; we rejected those points showing occasional spikes and also those immediately after the change in the position of the radiometers. The data were then binned in  $4^\circ$  RA intervals and the differences in Eq. (4) were calculated with their statistical errors.

In order to increase information about the synchrotron spectral index, we compared our data with two sky surveys: the map at 408 MHz of Haslam et al. (1982) and the map at 1420 MHz of Reich & Reich (1986).

Section 3.1 describes data analysis, while Section 3.2 describes the procedure we used to make the maps comparable with our data.

#### 3.1 Differential profiles and corrections

The WM experiment was designed to have similar antenna beams for all the radiometers (see Table 1). For a comparison of data taken at different frequencies, we corrected the profiles in order to “normalize” the different antennas responses to our average antenna beam (Half Power Beam Width =  $18^\circ$ ). We generated a “synthetic” sky by scaling to our frequencies and convolving with the radiometers beam the full-sky 408 MHz Haslam et al. map and a catalogue of 7400 HII sources at 2.7 GHz (Witebsky 1978). We then calculated for every RA bin  $a$  in the profiles the coefficient  $\eta$  to convert the measured signal into a signal corresponding to an antenna with  $18^\circ$  HPBW:

$$\eta(a) = \frac{T_{18^\circ}(a)}{T_{\text{HPBW}}(a)} \quad (7)$$

For the points of the differential profile, this translates into the conversion coefficient:

$$\eta_{diff} = \frac{\Delta T_{18^\circ}}{\Delta T_{\text{HPBW}}} \quad (8)$$

where

$$\Delta T_{18^\circ} = T_{18^\circ}(a) - T_{18^\circ}(b) = T_{\text{HPBW}}(a)\eta(a) - T_{\text{HPBW}}(b)\eta(b) \quad (9)$$

where  $a$  and  $b$  are generic sky bins whose separation (in RA) is  $38^\circ$  (in fact, observations of points at  $15^\circ$  from the zenith, carried out at a terrestrial latitude of  $38^\circ$ , correspond to points at  $19^\circ$  from the zenith and declination of  $36^\circ$  on the celestial sphere). Because all the instruments have similar antenna beams, the coefficient  $\eta_{diff}$  typically varies in the range 0.8-1, thus giving rise to small corrections to the data.

After this correction, the resulting Galactic profiles are directly comparable and are shown in Figs. 2a-2d. Note the decreasing signal-to-noise ratio with increasing frequency due to the spectral behaviour of the synchrotron spectral index (Eq. (2)).

Because the main goal of this work is to evaluate a mean synchrotron spectral index in the observed sky region, for all the profiles the bremsstrahlung contribution has been evaluated using the catalogue of HII sources, convolved with the  $18^\circ$  “standard” antenna beam and scaled at the observation frequencies with a spectral index  $\alpha_{ff} = 2.1$  (Scheffler & Elsässer, 1987). This component has been subtracted leaving the synchrotron component as a result (see Section 4.1 for systematic errors arising from the subtraction).

#### 3.2 The Maps

The 408 MHz Haslam map is a full-sky survey composed from several data sets at the same frequency obtained using different telescopes with similar beam size; the final angular resolution is  $0.85^\circ$ . The 1420 MHz Reich & Reich map covers declinations  $\delta > -19^\circ$  and the angular

resolution is  $0.6^\circ$ . From these surveys we extracted the Galactic profiles, corresponding to our observed sky region, convolved them with a gaussian beam with HPBW =  $18^\circ$ , and then constructed the differential profiles by simulating the observation strategy; the profiles are shown in Figs. 2e and 2f. These two surveys have intrinsic uncertainties in zero level and gain calibration, the first not affecting our analysis because of the differential reduction technique. The gain calibration error is 10% for the 408 MHz map and 5 % for the 1420 MHz one; these errors have been added in quadrature to the statistical errors in both map profiles.

The two maps are in total intensity, while our instruments were sensitive only to one linear polarization; to make our data and the maps directly comparable we corrected the maps using the linear polarization survey of the Galactic background from Brouw & Spoelstra (1976) convolved with the  $18^\circ$  beam. We subtracted from the profiles the component perpendicular to the polarization direction of our instruments. The polarization data have a statistical mean error of 0.34 K for the 0.408 GHz data and 0.06 K for 1.4 GHz. We included these errors as statistical errors. Finally, the maps, as well as the data, have been corrected for the HII contribution and errors arising from this procedure were considered.

## 4 Results and Error Analysis

In order to evaluate the synchrotron spectral index we produced temperature-temperature plots, or “TT-plots”. Such plots display as ordinate and abscissa antenna temperatures measured simultaneously at two different frequencies on the same region of the sky. TT-plots were made for every pair of frequencies between data and maps, excluding 1.375-1.55, 1.375-1.42, 1.42-1.55 GHz, because they are too close to obtain a meaningful result, and 3.8-7.5 GHz for the big errors due to the decreased signal-to-noise ratio. In Fig. 3 all the TT-plots are shown; the resulting synchrotron spectral indices are listed in Table 2 with final errors, including the systematic effects discussed in Section 4.1. Note the excellent agreement of the results obtained using our low frequencies (1.375 and 1.55 GHz) and the 1.42 GHz map, which confirms that our data don’t have unexpected systematic problems. The slope of the best fit to the data,  $m$ , gives the synchrotron spectral index:  $\alpha = \log(m)/\log(\nu_1/\nu_2)$ , where  $\nu_1$  and  $\nu_2$  are the frequencies of the two sets of data. Table 4 shows the statistical parameters of the TT-plots. Fig. 4 shows all our results; the spectral indices are evaluated between the frequency indicated in the box and the one on the x-axis. The more significant contribution to the evaluation of  $\alpha$  comes from data taken in the region close to the Galactic plane, because they have a large range of temperature and thus weigh the most in the fit. Thus we can say that our results are primarily representative of synchrotron emission from the Galactic plane.

### 4.1 Evaluation of Systematic Effects

For each of the effects considered in this paragraph, we calculate with the TT-plot the spectral index for data with and without a given effect; the difference between the two spectral indices is the induced systematic error on  $\alpha_{syn}$  and we list them in Table 3. In our analysis, we evaluated all the second order effects producing systematic errors; the discussion is divided in two parts, the first one dedicated to effects due to the corrections in the Galactic profiles, and the second one devoted to the evaluation of instrumental effects.

We considered the possibility that our HII catalogue was not complete and we evaluated the effect of this incompleteness on the results. For this purpose we corrected our data with an earlier catalogue of only 900 HII sources and evaluated  $\alpha_{syn}$ : the typical value of the resulting error is  $\sigma_{\alpha_{syn}} \sim 2\%$ , as shown in Table 3. We took into account also the effect produced by an error on the free-free spectral index, considering values  $\alpha_{ff} = 2.10 \pm 0.05$ ,

obtaining typically a percentage error of  $\sigma_{\alpha,ind,ff} \sim 1\%$ . We also evaluated all the indices without the subtraction of the HII component: the typical difference between these indices and the corrected ones is 0.3. We estimate that in the worse case the HII compilation would have 20 % error resulting in an error of  $\sim 0.06$  in the spectral indices which would not change the results significantly.

Instrumental effects can arise from uncertainties on the beam pattern configuration, errors in the pointing direction, variations of atmospheric emission and from the possible change of the instrument response when tipped between pointing directions. It is important to point out that, for the differential reduction technique we used, an effect that is constant in time or in sky position would not affect the estimate of spectral index; in fact, adding a constant value to the data set of an instrument would not change the slope of the fit that is used to calculate  $\alpha_{syn}$ . An example of constant differential signal is the ground contribution, which has not been considered in the analysis.

The uncertainty in the Half Power Beam Width, that has been measured during the experiment, is  $\pm 2^\circ$ . To evaluate the error on  $\alpha_{syn}$  we used the synthetic sky at each frequency convolved with the nominal beams of the experiment (HPBW =  $16^\circ, 17^\circ, 18^\circ, 21^\circ$ ) and with the same beams but with  $\pm 2^\circ$  in the HPBW. The resulting changes in  $\alpha_{syn}$  are the errors listed in Table 3 ( $\sigma_{\alpha,beam} \lesssim 1\%$ ).

The measured uncertainty in the pointing directions is  $\lesssim 30'$ . We made the TT-plot with the Haslam differential profile resulting from two simple profiles at distance  $29^\circ$  in RA (instead of  $30^\circ$ ). The difference between the values of  $\alpha_{syn}$  with these two different displacements in RA was calculated for every TT-plot with 408 MHz data; a mean percentage error ( $\sigma_{\alpha,poin} = 0.1\%$ ) is obtained.

Fig. 5 shows correlations between data taken in different days for the frequencies we analysed; the correlation is very good for the radiometer at lowest frequency (1.375-1.55 GHz) and less for the 3.8 GHz one. To evaluate the effect of data non-repeatability, for each pair of frequencies we made two TT-plot with data registered September 6th and 8th; with the differences between each pair of  $\alpha_{syn}$  we evaluate a mean percentage error on the synchrotron spectral index (2%). The origin of this effect could be due to the radiometer position dependence but this may arise also from variations of atmospheric emission. While the water vapor contribution is very small at these frequencies, the overall atmospheric radiation varies with position and time for changes in pressure profiles (Bersanelli et al. 1995) in a way compatible with the observed variation in our data. We include this effect in  $\sigma_{\alpha,atm}$ .

The uncertainty on the calibration coefficient  $G$  was also considered; the nature of the resulting error is statistical because it is dominated by the uncertainty on the registered value of the ambient temperature. In Table 3 (typical range  $\sim 2-5\%$ ) this component is included in the statistical data errors.

## 5 Discussion

We used our results to study the behaviour of the synchrotron spectral index with frequency and evaluate a mean synchrotron spectral index in the frequency region of this experiment (Section 5.1 and 5.2). The frequency dependence is consistent with that expected from the steepening of the Galactic cosmic rays electron spectrum. In addition, we compared the Haslam map with a map at high frequency (19 GHz) to point out the consistent spatial variation of  $\alpha_{syn}$  (Section 5.3).

## 5.1 Frequency Variation

As discussed in Section 1, synchrotron radiation arises from cosmic ray electrons; the interstellar energy spectrum does not have a constant slope, but steepens at an energy of  $\sim 10\text{-}20$  GeV. In fact cosmic ray electrons lose energy with different mechanisms: at energies  $\lesssim 10\text{-}20$  GeV they escape from the Galaxy, for  $E \gtrsim 10\text{-}20$  GeV the prevalent mechanism is synchrotron radiation. Because of the two combined effects, the equilibrium spectrum of the electrons changes its slope in this energy range (Webber 1983) corresponding to a frequency  $\sim 10$  GHz. Consequently, the synchrotron spectral index  $\alpha_{syn}$ , that is related with the electrons spectral index  $\delta$ , increases with increasing frequency (Lawson al 1987, Banday & Wolfendale 1990 & 1991). The results of our analysis (Fig. 4) suggest an initial increase of  $\alpha_{syn}$  corresponding to our higher frequency 7.5 GHz, although with a relatively poor signal-to-noise ratio. At lower frequencies the spectrum is more flat, as we expect. In Fig. 6 we compare our results with the few other published results in our frequency range and at higher frequencies and the trend seems to be confirmed.

## 5.2 Evaluation of a Mean Synchrotron Spectral Index

In the frequency range of our measurements, it is possible to evaluate a mean synchrotron spectral index in the observed sky region, since there is not an evident steepening until higher frequencies. A mean  $\alpha_{syn}$  between 1.4 and 3.8 GHz has been estimated using the results from the three TT-plots between 1.375, 1.550, 1.42 and 3.8 GHz, as the most statistically significant; the result is  $\alpha_{syn} = 2.76 \pm 0.09$ . Next, we calculate the spectral index using all the results, by a weighted mean of the indices derived with the TT-plots; this is less statistically meaningful because of some redundant information coming from different TT-plot (for example the TT-plot between 1.375 and 7.5 and the one between 1.375 and 3.8 cover partially the same frequency region) but it gives good information on the behaviour of  $\alpha_{syn}$  in a larger frequency range. For each index, the error in the weighted mean is the quadratic sum of statistical plus pointing and beam errors (the last two errors have an independent effect on the TT-plots). On the other hand, polarization, HII and atmosphere errors were considered as systematic, since the effects they have on the different evaluations of  $\alpha_{syn}$  are not independent. The mean  $\alpha_{syn}$  using only our data yields  $\alpha_{syn} = 2.81 \pm 0.16$ ; adding data from the 0.408 and 1.42 GHz maps, we derive  $\alpha_{syn} = 2.76 \pm 0.11$ .

## 5.3 Spatial Variation

As we said in Section 1.1, the synchrotron spectral index has also a consistent spatial variation due to changes in the electron spectrum and density and in the magnetic field intensity with the position in the sky (Eq. (3)). As an example, Fig. 7 is a plot of data from the Haslam map versus data from a preliminary 19 GHz map (Cottingham 1987; Boughn et al. 1990); the best fit line to data yields an estimate of  $\alpha_{syn} = 3.01$ . However there is a large range of possible values of  $\alpha_{syn}$  compatible with the dispersion of the data; much of the dispersion appears to be correlated with large angular scale spectral variation. We point out this behaviour of  $\alpha_{syn}$  in Fig. 8, where we show the ratio between the two maps; more precisely, if  $T_1(i)$  is the temperature of the  $i$ -th pixel in the 408 MHz map and  $T_2(i)$  the temperature of the same pixel at 19 GHz, the ratio map shows

$$ratio = \frac{T_2(i)}{T_1(i)} (\nu_2/\nu_1)^{\alpha_{syn}} \quad (10)$$

where we fixed  $\alpha_{syn}$  to a mean value of 2.8. Then, if the synchrotron spectral index changes from this mean value, the pixel color in the map changes too; an increase in  $\alpha_{syn}$  makes

color black, a decrease leads to red. One can recognize the feature of the North Polar Spur, where the synchrotron spectral index is steeper than the average (Lawson et al. 1987, Reich & Reich 1988). A part from this feature, the spectrum is flatter than the average at high galactic latitudes. This is in agreement with Reich & Reich (1988): they found a flattening of the spectrum with increasing latitude in the outer Galaxy direction and also, some evidence for a similar effect in the inner Galaxy direction (even if only the North Hemisphere data are currently available). Also Bloemen et al. (1993) found an hardening of the gamma-ray spectrum with latitude that translates into a flattening in the radio spectrum. The reason for the hardening of gamma-ray is still unclear since, from a simple diffusion model of the cosmic rays (Ginzburg & Syrovatskii 1964), a spectral steepening with latitude is expected. More complex models (e.g. Reich & Reich 1988, Bloemen et al. 1989) such as halo model may explain the observed effect with a competition of many different mechanisms (spatial diffusion, convection, adiabatic deceleration and energy losses), but the situation is very complex and need more data and modeling. Finally, we calculated the synchrotron spectral index between the two maps in the sky region of our experiment  $\alpha_{syn} = 3.00 \pm 0.20$ , as shown in Fig. 6. The 19 GHz map is a preliminary map, thus the ratio between 19 and 0.408 GHz only gives an indication of the synchrotron spectral index spatial variation in that frequency range, because of the residual errors in the preliminary 19 GHz data.

## 6 Conclusions

We have analysed data taken as part of an experiment dedicated to the measurement of the low-frequency spectrum of the Galactic continuous emission. The radiometers, operating at 1.375, 1.55, 3.8 and 7.5 GHz, observed a sky region at declination  $38^\circ$ . The differential reduction technique has allowed us to cancel the first order contributions from all the isotropic and symmetrical signals received by the radiometers, leaving the Galactic signal. In order to evaluate the synchrotron spectral index  $\alpha_{syn}$ , we have subtracted from the data the HII component derived from an HII sources catalogue. We have used the TT-plots to calculate the synchrotron spectral index and to evaluate systematic errors (arising from uncertainties in HII contribution, beam pattern configuration, pointing direction and atmospheric emission); we have compared our data with the Haslam and Reich & Reich maps to yield an estimate of  $\alpha_{syn}$  in the frequency range 0.408-7.5 GHz and primarily in the region of the Galactic plane. The general behaviour of  $\alpha_{syn}$  in this frequency range suggests a steepening of the synchrotron radiation spectrum at frequency  $\sim 10$  GHz, already visible at our higher frequency 7.5 GHz. The mean value of the synchrotron spectral index is  $2.81 \pm 0.16$  in the frequency range of this experiment (1.375-7.5 GHz) and  $2.76 \pm 0.11$  including the two maps.

As Fig. 6 shows, it is important to acquire new accurate sets of data in the frequency range 1-50 GHz to understand the frequency behaviour of the synchrotron spectral index. In particular, high sensitivity maps of extended regions of the Galaxy at sub-degree angular resolution will be extremely important in the context of the next generation of CMB experiments, such as the two planned space missions MAP and PLANCK Surveyor.

## Acknowledgments

We thank L.Danese, E. Gawiser and C. Paizis for useful discussions and suggestions; we also thank J. Aymon for his technical support. This work was funded in part by the Collaborative Research Grant CRG960175 of NATO International Scientific Exchange Program and by the Director, Office of Energy Research, Office of High Energy and Nuclear Physics, Division of High Energy Physics of the U.S. Department of Energy under contract DE-AC03-76SF00098.

**Table 1**  
**Radiometers and Observations parameters**

<i>Frequency [GHz]</i>	<i>Measured Sensitivity</i>	<i>HPBW<sup>a</sup></i>	<i>Date (1988)</i>	<i>RA [h]</i>
1.375-1.550	18 mK Hz <sup>-1/2</sup>	18° - 16°	6 Sep	0-4.3 18.3-24
			8 Sep	0-5 19-24
3.8	13 mK Hz <sup>-1/2</sup>	17°	6 Sep	0-4.3 18.3-24
			8 Sep	0-5 20.3-24
			10 Sep	21-23
7.5	44 mK Hz <sup>-1/2</sup>	21°	6 Sep	0-2.3 18.3-24
			8 Sep	0-5 19-21
			10 Sep	21-23

a) The HPBW of the gaussian beam that approximates the real one

**Table 2**  
**Spectral indices and errors**

<i>Frequencies [GHz]</i>	$\alpha_{syn}$	$\sigma_{\alpha,tot}$
0.408 - 1.375	2.775	0.095
0.408 - 1.42	2.776	0.119
0.408-1.55	2.691	0.093
0.408 - 3.8	2.731	0.079
0.408 - 7.5	2.951	0.163
1.42 - 3.8	2.681	0.152
1.42 - 7.5	3.057	0.252
1.375 - 3.8	2.689	0.117
1.375 - 7.5	3.327	0.372
1.550 - 3.8	2.841	0.110
1.550 - 7.5	3.609	0.508

**Table 3**  
**Statistical and Systematic Errors [K]**

<i>Frequencies [GHz]</i>	$\sigma_{\alpha,stat}$	$\sigma_{\alpha,beam}$	$\sigma_{\alpha,poin}$	$\sigma_{\alpha,ind.ff}$	$\sigma_{\alpha,ff}$	$\sigma_{\alpha,atm}$	$\sigma_{\alpha,pol}$
0.408 - 1.375	0.064	0.032	0.003	0.017	0.025	0.055	0
0.408 - 1.42	0.100	-	-	0.033	0.003	0.055	0.001
0.408 - 1.550	0.060	0.039	0.003	0.012	0.022	0.054	0.001
0.408 - 3.8	0.041	0.025	0.003	0.007	0.029	0.055	0
0.408 - 7.5	0.130	0.002	0.003	0.049	0.062	0.059	0
1.42 - 3.8	0.120	0.026	0.003	0.034	0.062	0.054	0
1.42 - 7.5	0.274	0.006	0.003	0.068	0.123	0.064	0
1.375 - 3.8	0.061	0.07	0.003	0.036	0.028	0.054	-
1.375 - 7.5	0.320	0.001	0.003	0.120	0.129	0.066	-
1.550 - 3.8	0.069	0.039	0.003	0.035	0.033	0.057	-
1.550 - 7.5	0.440	0.004	0.004	0.158	0.185	0.072	-

**Table 4**  
**Statistics**

<i>Frequencies [GHz]</i>	$\chi^2_{\nu}$	$r_S$	$N_{points}$
0.408-1.375	0.322	0.916	38
0.408-1.55	0.404	0.874	38
0.408-3.8	0.620	0.911	38
0.408-7.5	2.574	0.272	38
0.408-1.42	0.031	0.972	38
1.42-3.8	0.396	0.856	38
1.42-7.5	2.549	0.252	38
1.375-3.8	0.956	0.789	38
1.375-7.5	2.736	0.212	38
1.55-3.8	0.917	0.757	38
1.55-3.8	2.787	0.190	38

**Table 5**  
**Other evaluations of  $\alpha_{syn}$**

<i>Frequency range [GHz]</i>	$\alpha_{syn}$	HPBW	<i>Reference</i>	<i>Notes</i>
0.408-2	$2.65 \pm 0.05$	$14^\circ$	Bersanelli et al. 1995	$-40 \leq \delta \leq -60$
0.408-31.5	$\geq 2.9$	$7^\circ$	Kogut et al. 1996 <sup>a</sup>	full sky
1.42-5	$2.9 \pm 0.3$	$2^\circ$	Bersanelli et al. 1996	
1.42-10.4	3.4	$5^\circ$	Bersanelli et al. 1996	
1.42-14.9	3.0	$5^\circ$	Bersanelli et al. 1996	

a) We independently estimated the spectral index between 0.408 and 31 GHz yielding the same result.

## References

- Anday, A. J. & Wolfendale, A. W. 1990, *MNRAS*, **245**, 182.
- Anday, A. J. & Wolfendale, A. W. 1991, *MNRAS*, **248**, 705.
- Ansadoun, M. et al. 1993, *ApJ*, **409**, 1.
- Arsanelli, M. et al. 1995, *Astro. Lett. and Communications*, **32**, 7.
- Arsanelli, M. et al. 1995, *ApJ*, **448**, 8.
- Arsanelli, M., Bouchet, F.R., Efstathiou, G., Griffin, M., Lamarre, J.M., Mandolesi, N., Nordgaard-Nielsen, H.U., Pace, O., Polny, J., Puget, J.L., Tauber, J., Vittorio, N., Volonte', S. 1996, *COBRAS-SAMBA: report on the phase A study*, ESA.
- Boelmen, H. et al. 1993, *Astron. Astrophys.*, **267**, 372.
- Broughn, S. P. et al. 1990, *Rev. Sci. Instr.*, **61**, 158.
- Brouw, W. N. & Spoelstra, T. A. Th. 1976, *Astron. Astrophys. Suppl. Ser.*, **26**, 129.
- Bottingham, D. A. 1987, *PhD thesis*, Princeton Univ.
- De Amici, G. et al. 1990, *APJ*, **359**, 219.
- Finzbug, V. L. & Syrovatskii, S. I. 1964, *The origin of the Cosmic Rays*, Oxford, Pergamon Press.
- Haslam, C. G. T. et al. 1982, *Astron. Astrophys. Suppl. Ser.*, **47**, 1.
- Gogut, A. et al. 1990, *ApJ*, **355**, 102.
- Gogut, A. et al. 1996, *ApJ*, **460**, 1.
- Hawson, K. D. et al. 1987, *MNRAS*, **225**, 307.
- Reich, P. & Reich, W. 1986, *Astron. Astrophys. Suppl. Ser.*, **63**, 205.
- Reich, P. & Reich, W. 1988, *Astron. Astrophys. Suppl. Ser.*, **74**, 7.
- Scheffler, H. & Elsässer, H. 1987, *Physics of the Galaxy and Interstellar Matter*, Springer-Verlag, Heidelberg.
- Sommers, G. F. et al. 1985, *ApJ Lett.*, **291**, L23.
- Webber, W. R. 1983, in *Composition and origin of cosmic rays; Proceedings of the Advanced Study Institute*, Erice, Italy, June 20-30, 1982, Dordrecht, D. Reidel Publishing Co., 83.
- Whitehead, C. 1978, not published.

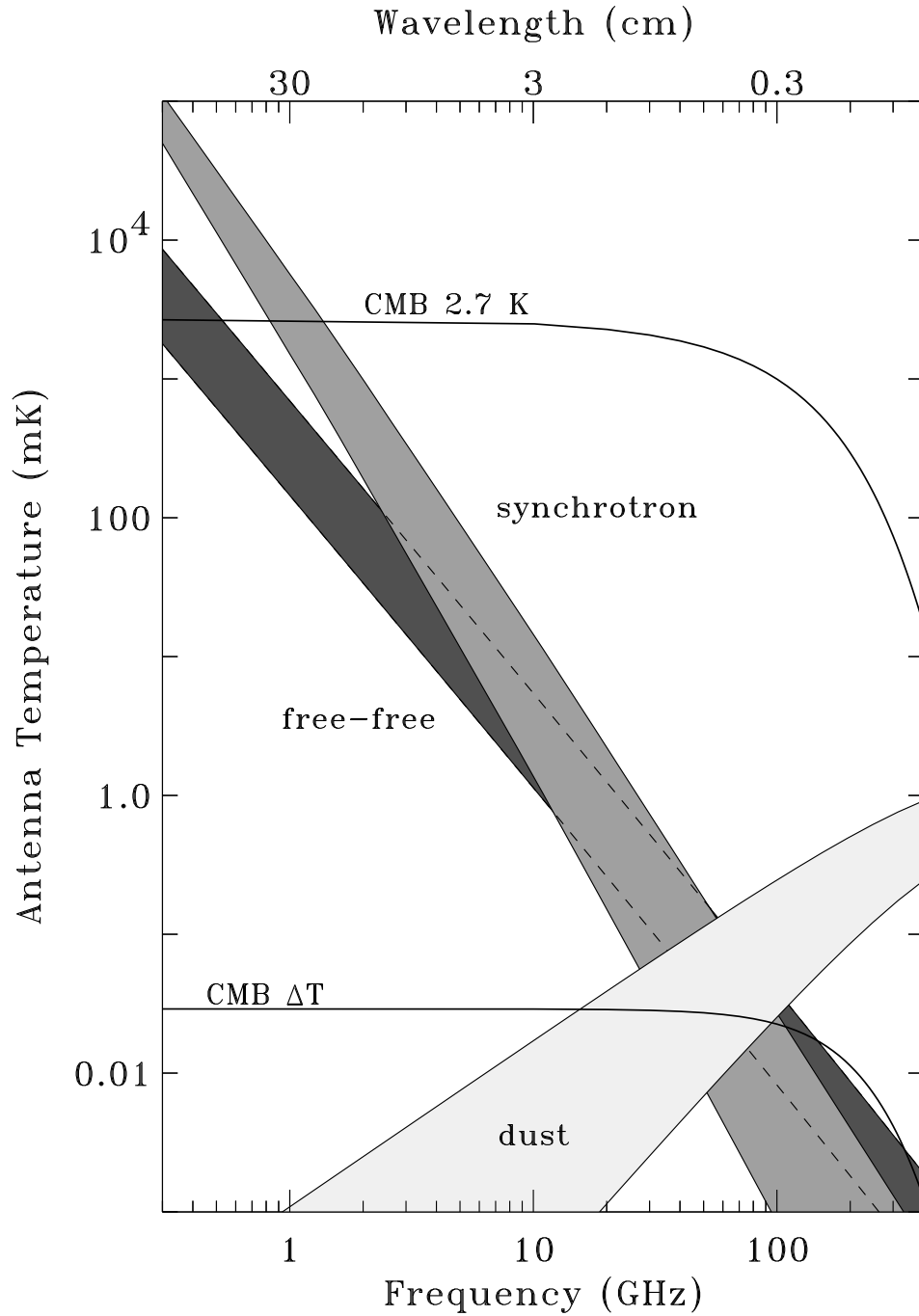
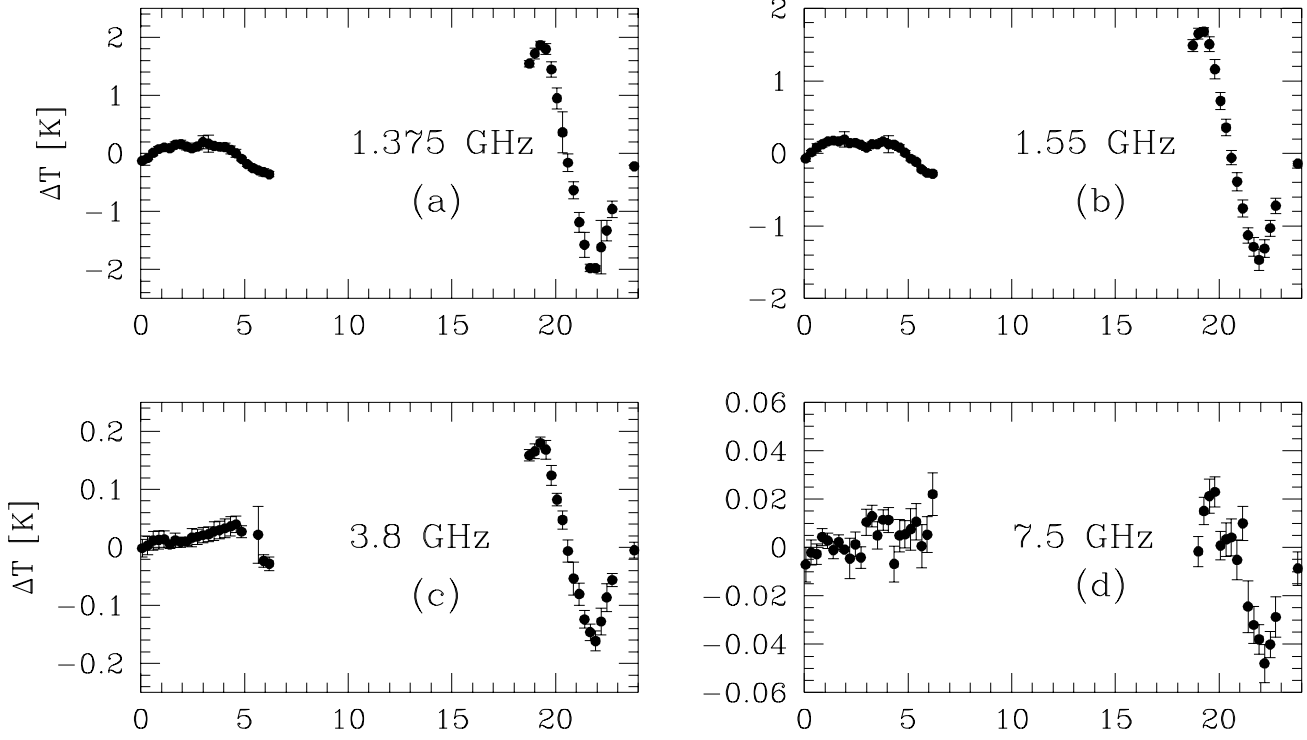


Figure 1: Galactic emission components and CMB spectra for moderate angular resolution ( $7^\circ$  HPBW) and galactic latitude  $|b| < 20^\circ$ . The shaded regions indicate the range of synchrotron, free-free and dust emission. Solid lines indicate the mean CMB spectrum and rms amplitude of anisotropy.

our data



the maps

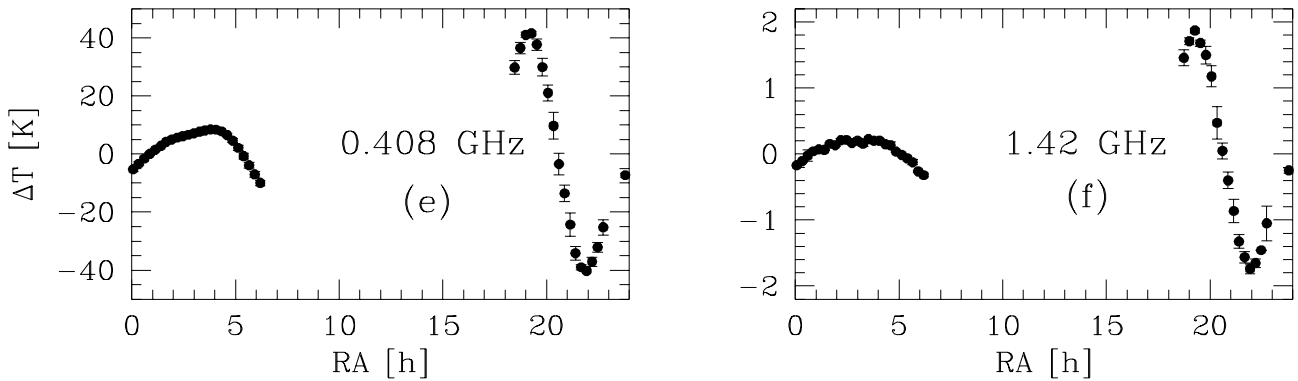


Figure 2: All profiles. Figs 2a-2d: Differential Galactic profiles derived from our data at the frequencies indicated in the plots. Figs 2e-2f: Differential Galactic profiles derived from the maps at 408 and 1420 MHz.

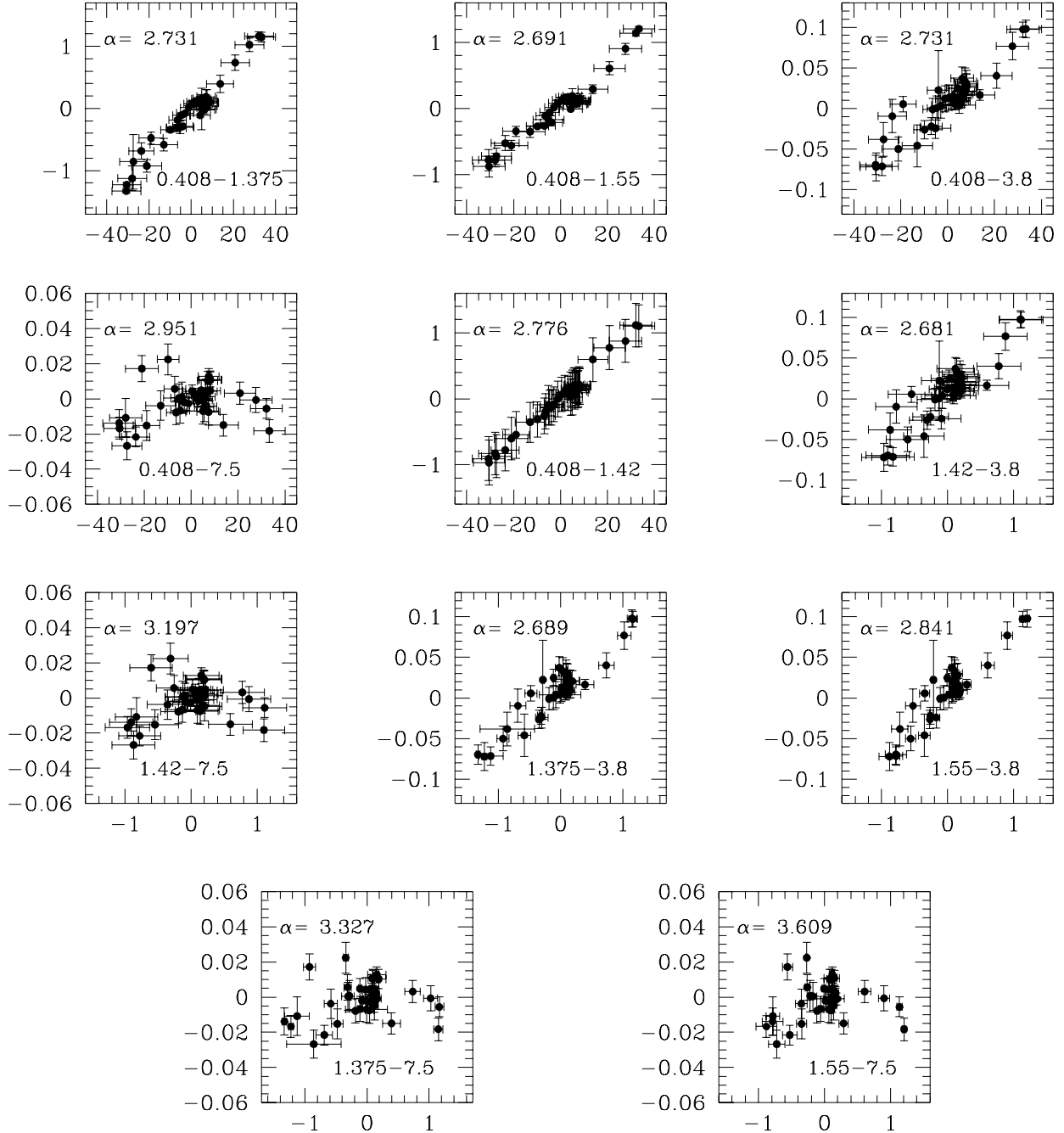


Figure 3: All the  $TT$ -plots are shown. The resulting synchrotron spectral index is indicated in every plot, as well as the pair of frequencies (GHz) at which data have been taken, the first referring to abscissa and the second to ordinate. The units are K on both axis.

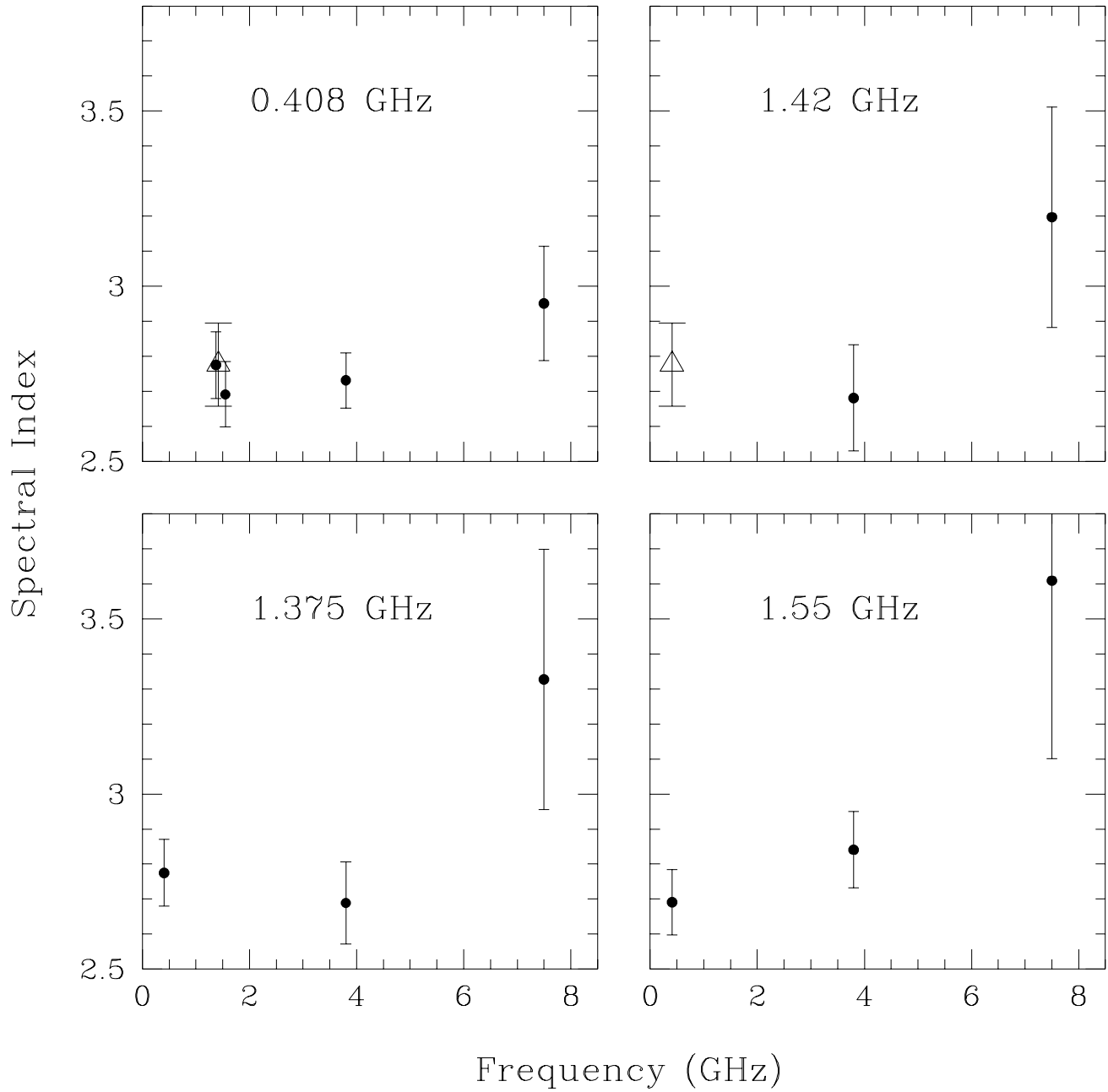


Figure 4: In each box the spectral indices between the frequency indicated in the box and the frequencies on the x-axis are shown. The triangle point refers to our evaluation of the synchrotron spectral index between the two maps.

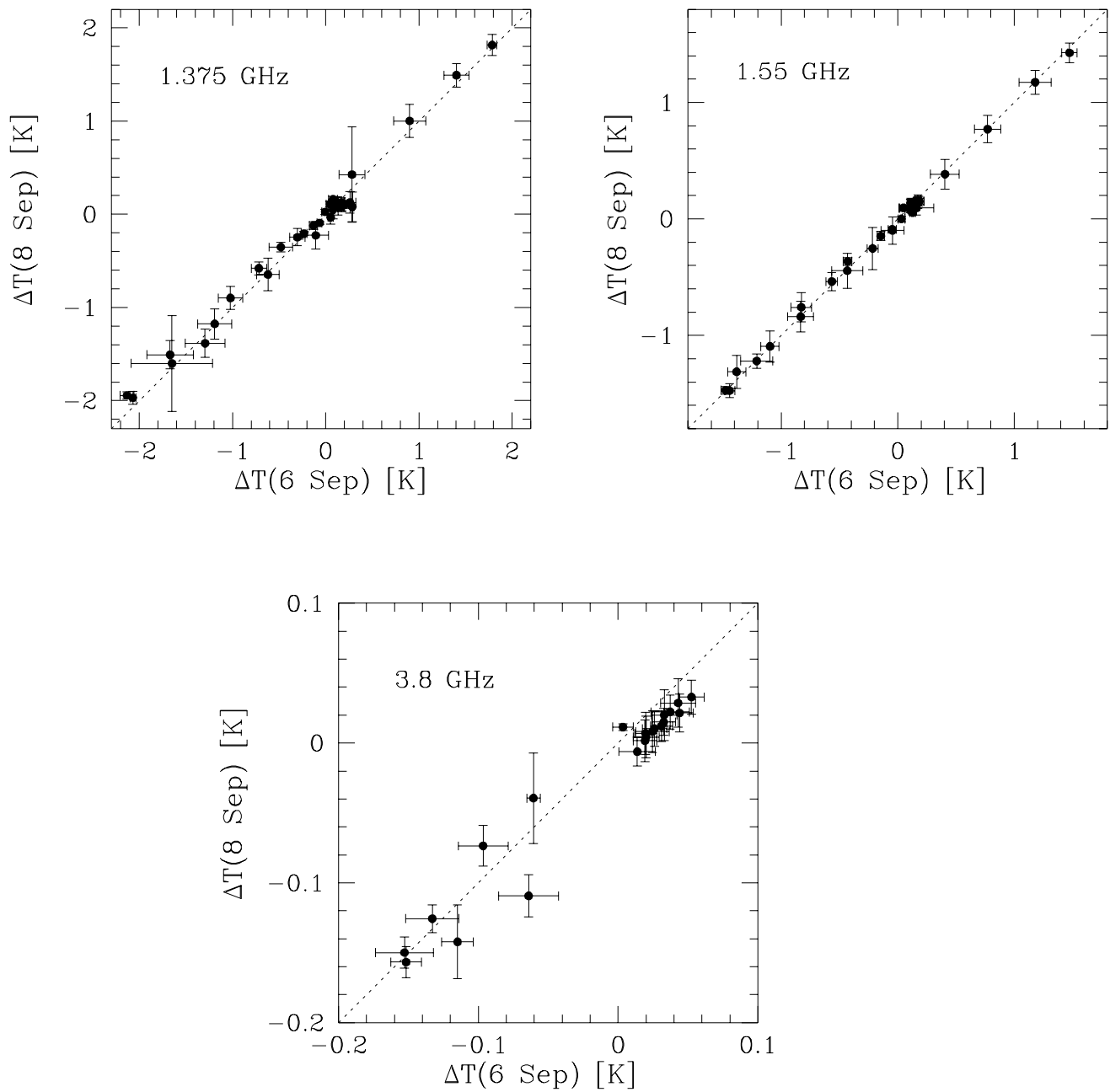


Figure 5: *Correlations between data taken in different days: on the x-axis data taken on the 6th of September are plotted, while on the y-axis, those taken on the 8th.*

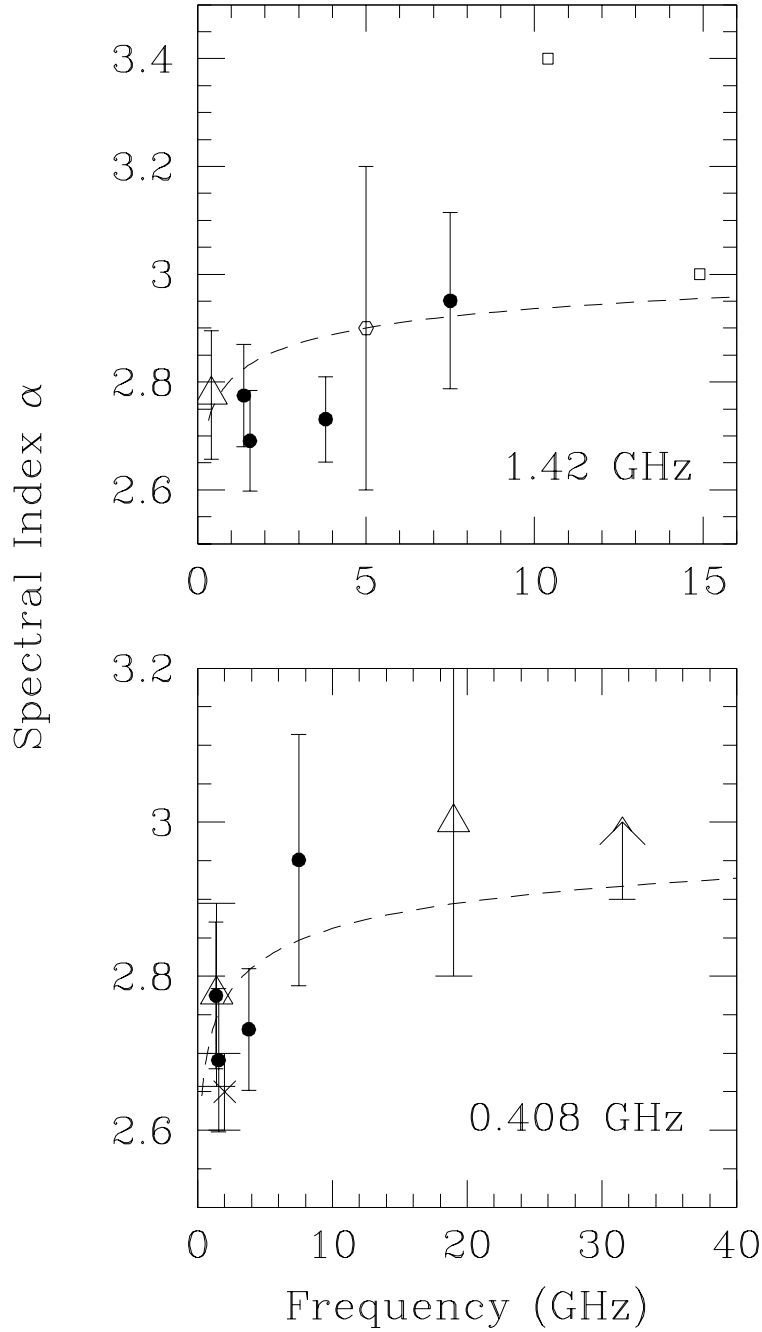


Figure 6: Spectral indices derived in this work are compared with other published estimates. The indices are between 1.42 GHz and frequencies on the x-axis in the upper plot and between 0.408 GHz and frequencies on the x-axis in the lower plot. Full circles: this work. Empty triangles: our evaluations of  $\alpha_{syn}$  from the maps at 0.408, 1.42 and 19 GHz. See Table 5 for other points's references. The smoothed dashed lines are naive calculation of the spectral index based on the local cosmic ray electron spectrum.

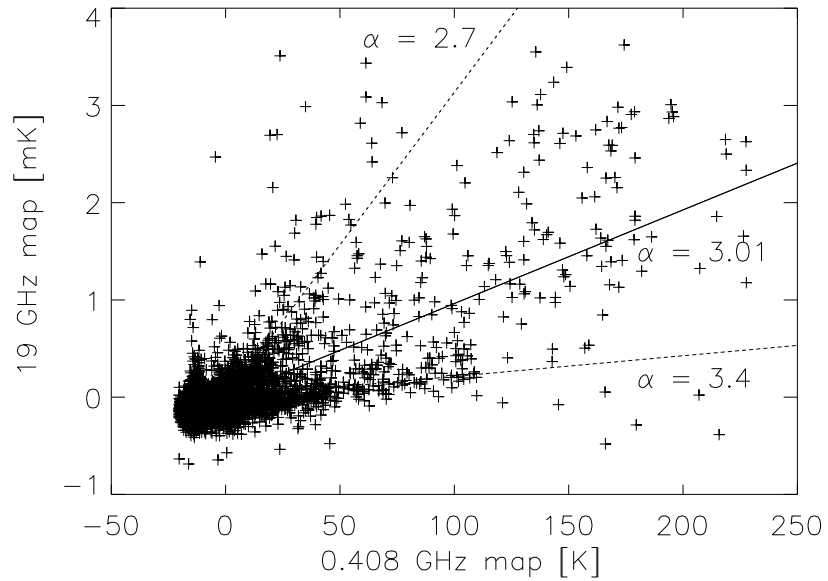


Figure 7: *TT*-plot with all-sky data from 408 MHz and 19 GHz maps. In the plot best fit to data is shown (solid line) and upper and lower limits (dashed lines) to possible spectral index values. An offset has been subtracted to 19 GHz data; some data have negative values because the mean has been subtracted to calculate the best fit.

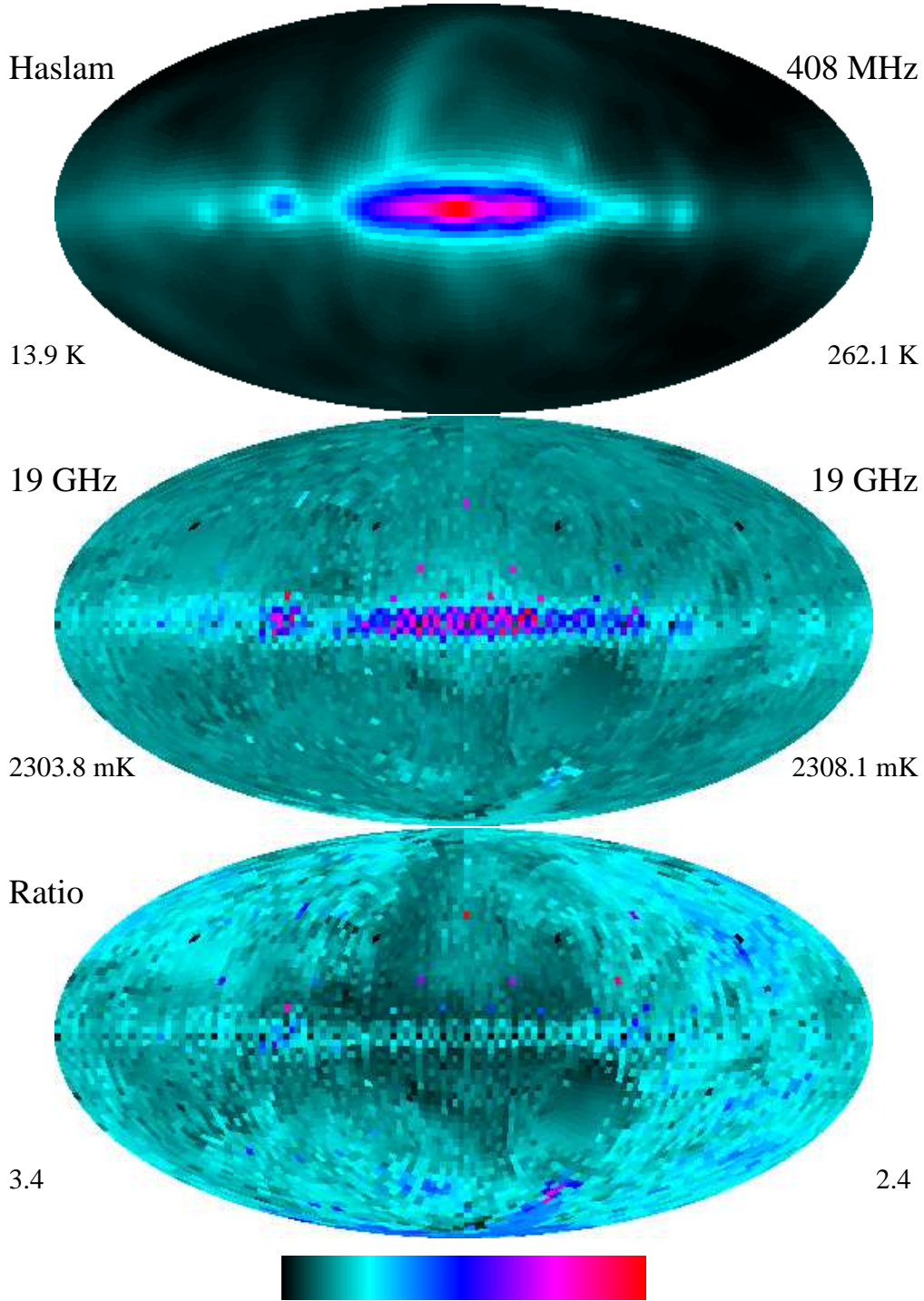


Figure 8: *Top: Haslam et al. 408 MHz full-sky map. The minimum and maximum temperatures are labeled at the bottom of the map. Middle: preliminary 19 GHz map (Cottingham 1987, Boughn et al. 1990). The two smoothed regions (one in the southern hemisphere on the right, the other one in the northern hemisphere on the left) are not covered by the survey and the blank pixels have been replaced with the average temperature from surrounding regions. The minimum and maximum temperature at the bottom include the offset of the survey. Bottom: Ratio map between the 0.408 and 19 GHz maps. The bottom labels refer to the maximum and minimum spectral index.*